SLAC-PUB-2187
August 1978
(T/E)

BOUND STATE AND PERTURBATIVE QCD EFFECTS IN LEPTON PAIR PRODUCTION*

Christopher M. Debeau
Department of Physics, University of California
Irvine, California 92717

Dennis Silverman
Stanford Linear Accelerator Center
Stanford University, Stanford, CA 94305

and

Department of Physics, University of California
Irvine, California 92717

ABSTRACT

In this paper we compare the bound state or constituent interchange model and perturbative QCD contributions to lepton pair production. We improve the CIM model with explicit one-gluon exchange calculations of bound state effects and use a general gauge invariant amplitude. We also use off mass shell kinematics to provide finite results at zero momentum transfer. Recent lepton pair data in transverse momentum $Q_\perp$ is fit predominantly with the CIM contribution, with consistent normalization to other CIM processes. The emergence of the QCD contribution at larger $Q_\perp$ and higher energy is also studied.

(Submitted to Phys. Rev.)

*Supported in part by the National Science Foundation and the Department of Energy under contract no. EY-76-C-03-0515.

I. INTRODUCTION

In this paper we study the non-perturbative bound state effects in lepton pair production with the constituent interchange model (CIM).[1,2] We also study the lowest order quantum chromodynamics (QCD) perturbation contribution[3] in a unified context with the non-perturbative effects. In the large $p_\perp$ pion spectra the CIM accounts for the $p_\perp^{-8}$ behavior[4,5] and the QCD canonical scaling contribution[6,7] for the $p_\perp^{-4}$ behavior at higher $p_\perp$. We have a similar situation in the lepton pair spectra.[1,2] Since we are calculating the transverse momentum ($Q_\perp$) distribution of the lepton pair we do not directly compute the collinear $Q_\perp$=0 Drell-Yan process, but include the dynamical sources of high $Q_\perp$ behavior in the CIM and QCD processes. This is done through the hard scattering expansion.[8]

In the bound state CIM contributions Fig. 1, the scaling behavior of cross sections is multiplied by the extra form factor squared $g_M^2 m^2/(m^2-t)$. This results from the far off shell gluon exchange in the wave function that encompasses the size associated with the wave function or probability density near the origin as measured by $\langle 1/r \rangle$. In the hard scattering expansion[8] we have the initial particles in the wave function as nearly on shell but include the exchanged off shell gluon (Fig. 1) in the hard scattering cross section and integrate over the wave function.

The use of a qq or $q\bar{q}$ wave function in CIM is simply a way of representing the correlated sharing of the nucleon's momentum by the exchanged quark which emits the gluon and the quark which absorbs the gluon. It is described by an equivalent low mass scalar or pseudoscalar $q\bar{q}$ "meson" or qq "diquark" called M.

In this paper we first derive the spinor form for an off mass shell exchanged constituent antiquark from a bound state wave function for $M \to q\bar{q}$. Using the one gluon exchange impulse approximation the spinor form for the antiquark of momentum k is derived to be $mg_M \bar{u}(q')\not{k}/(k^2-m^2)$.

Starting with the t channel diagram Fig. 1(a) with the CIM spinor form, we then formulate the general gauge invariant amplitude for lepton pair production including non-perturbative effects in both the lepton pair mass Q^2 and crossed meson channel variable u.

We next include in the hard scattering processes the perturbative QCD diagrams which do not include extra gluon scatterings inside the hadron. We present the QCD $qG \to \gamma^* q$ Compton amplitudes and the annihilation $q\bar{q} \to \gamma^* G$ amplitude (Fig. 2) and associated cross sections where G is a gluon. These are of course scale invariant matrix elements.

The quark exchange diagrams in CIM and QCD perturbation both require cutoffs in that the near on shell quark exchanges lead to very sharp and experimentally unobserved rises for $Q_\perp < 1$ GeV. The bound state structure gives a natural cutoff by treating the incoming quarks, gluons, and effective mesons as spacelike virtual particles. This also expresses the color confinement of these constituents. It also suggests that since the cutoffs arise from the source of the constituents and not the particular hard scattering process, then the same cutoffs should be used for both the CIM and QCD contributions.

We then calculate the CIM and perturbative QCD contributions to the cross section together, using the same cutoffs. The CIM contributions dominate and the shape in $Q_\perp$ determines the mean off shell values of the constituent momenta. The perturbative QCD contributions are reduced

sharply from the non-cutoff calculation at small $Q_\perp$, but approach the non-cutoff calculations at $Q_\perp \gtrsim 3$ GeV/c. They are about one third of the cross section at $Q_\perp \simeq 4$ GeV/c. The QCD perturbation contributions dominate the CIM at $Q_\perp > 6$ GeV/c. This result is similar to the large $p_\perp$ single pion results where the scaling QCD contributions dominate the CIM[7] at $p_\perp \gtrsim 10$ GeV/c.

II. OFF SHELL q-$\bar{q}$ MESON VERTEX

We derive the off shell quark or antiquark form of the vertex ($|k^2| >> m^2$) in the impulse approximation with single gluon exchange (Fig. 3). We use the impulse approximation to treat the q and $\bar{q}$ in the wave function as on shell and have the off mass shell momentum carried by the gluon. The wave function times off shell scattering amplitude summed over spins for a pseudoscalar meson is (Fig. 3)

$$\bar{u}(p')F_M(k) = \left(\frac{4}{3}\right)\int \frac{d^4p}{(2\pi)^4}\,\psi(p,q;p_b)\frac{g^2}{(\Delta P)^2}\,\bar{u}(p')\gamma_\alpha(\not{p}+m)\gamma_5(-\not{q}+m)\gamma^\alpha \tag{2.1}$$

where 4/3 is the color factor and m is the quark mass. Commuting γ_5 and summing over α gives

$$\gamma_\alpha(\not{p}+m)(\not{q}+m)\gamma^\alpha = 2(p+q)^2 - 2m(\not{p}+\not{q}) = 2m_b^2 - 2m(\not{p}'-\not{k})$$

The gluon propagator evaluated with $p \simeq xp_b$

$$(\Delta P)^2 = -2p'\cdot p = -x2p'\cdot p_b = -x\left(k^2-m^2-m_b^2\right) \tag{2.2}$$

which allows us to factor out the $1/k^2$ due to the gluon propagator. Using $\not{p}'$ on $\bar{u}(p')$ we finally get

$$\bar{u}(p')F_M(k) = mg_M\,\bar{u}(p')\gamma_5\,\frac{\left(\not{k}+m-m_b^2/m\right)}{k^2-m^2-m_b^2} \tag{2.3}$$

where

$$g_M = \left(\frac{4}{3}\right) 2g^2 \int \frac{d^4p}{(2\pi)^4} \frac{\psi(p,q;p_b)}{x} \quad . \tag{2.4}$$

mg_M in Eq. (2.4) is not the wave function at the origin since it includes $1/x$. Since this arises from the gluon propagator, the dimensional factor mg_M is analogous to $\langle 1/r \rangle$ non-relativistically. Since we need Eq. (2.3) only to lowest order in $m/\sqrt{-k^2}$ we often abbreviate it as

$$\bar{u}(p')F_M(k) = mg_M \, \bar{u}(p') \, \gamma_5 \not{k}/k^2 \quad . \tag{2.5}$$

III. CIM CONTRIBUTION TO LEPTON PAIRS AND GAUGE INVARIANT AMPLITUDE

The quark exchange (t-channel) contribution to $qM \to \gamma^* q$ is shown in Fig. 1(a) and has the current

$$\mathcal{M}^t_\mu = \bar{u}(q')F_M(k) \frac{\not{k}+m}{k^2-m^2} \gamma_\mu \, u(q) \tag{3.1}$$

To leading order in m this is

$$\mathcal{M}^t_\mu \cong \frac{mg_M}{k^2-m^2} \bar{u}(q') \, \gamma_5\gamma_\mu \, u(q) \tag{3.2}$$

In order to make a gauge invariant current we must add general axial vector terms to (3.2), as done by Drell and Lee.[9] Isospin rotating to the neutral meson amplitude allows us to eliminate terms not having the same charge conjugation[9] as $\gamma_5\gamma_\mu$. This eliminates $\gamma_5(q+q')_\mu$, $\gamma_5(\not{q}+\not{q}')Q_\mu$, $\gamma_5(\not{q}+\not{q}')P_\mu$, $\gamma_5\not{Q}(q+q')_\mu$, $\gamma_5\not{P}(q+q')_\mu$, $\gamma_5[\not{Q},\gamma_\mu]$ and $\gamma_5[\not{P},\gamma_\mu]$. Using the Dirac equation on the spinors, to leading order in m, terms in $\gamma_5\not{P}$ become $\gamma_5\not{Q}$ and $\gamma_5[\not{q}+\not{q}',\gamma_\mu]$ becomes $2(q_\mu-q'_\mu)\gamma_5 = 2(Q_\mu-P_\mu)\gamma_5$. We are thus left with $\gamma_5 Q_\mu$, $\gamma_5 P_\mu$, $\gamma_5\not{Q}Q_\mu$, and $\gamma_5\not{Q}P_\mu$ as independent terms. With $u = (P-Q)^2 = Q^2 - 2P\cdot Q + m_b^2$ we write the general form conveniently for

$Q^2 >>$ mass^2 and $|u| >>$ mass^2 as

$$\mathcal{M}_\mu = \frac{mg_M}{k^2-m^2}\,\bar{u}(q')\gamma_5\left[\gamma_\mu - \frac{A\not{Q}Q_\mu}{Q^2} + \frac{B\not{Q}(2P-Q)_\mu}{Q^2-2P\cdot Q} - \frac{CQ_\mu}{Q^2} + \frac{D(2P-Q)_\mu}{Q^2-2P\cdot Q}\right]u(q) \tag{3.3}$$

Current conservation, $Q^\mu\mathcal{M}_\mu = 0$, and the independence of γ_5 and $\gamma_5\not{Q}$ then give two equations for their coefficients

$$1 - A - B = 0 \tag{3.4a}$$

$$C + D = 0 \tag{3.4b}$$

Since the C and D terms are independent of the t-channel pole contribution of $\mathcal{M}^t_\mu$ in (3.2), they are not required for gauge invariance, and for simplicity we take them to be zero. The A and B terms represent contributions of the general form of Fig. 1(b-c). We take $A = 1-\lambda$ and $B=\lambda$ for a final gauge invariant form

$$\mathcal{M}_\mu = \frac{mg_M}{k^2-m^2}\,\bar{u}(q')\gamma_5\left[\gamma_\mu - (1-\lambda)\frac{\not{Q}Q_\mu}{Q^2} + \lambda\frac{\not{Q}(2P-Q)_\mu}{Q^2-2P\cdot Q}\right]u(q) \tag{3.5}$$

The apparent pole at $Q^2=0$ is really the sum (seen at high Q^2) over several low mass intermediate states in Q^2 and similarly for the apparent pole at $u-m_b^2 = Q^2-2P\cdot Q$.

The CIM matrix element $\mathcal{M} = \epsilon^\mu(Q)\,\mathcal{M}_\mu$ squared and summed over spins with s, t, and u referring to the $q+M \to \gamma^*+q'$ subprocesses is

$$\Sigma|\mathcal{M}|^2 = \frac{m^2g_M^2}{(t-m^2)^2}\left\{-4u + 2\left(-\frac{st}{Q^2} + m_b^2\right)\left[(1-\lambda)^2 + \frac{\lambda^2Q^2\left(Q^2-4m_b^2\right)}{\left(u-m_b^2\right)^2} + \frac{4\lambda Q^2}{m_b^2-u} - \frac{2\lambda(1-\lambda)Q^2}{m_b^2-u}\right]\right\} \tag{3.6}$$

IV. QCD PERTURBATION PROCESSES FOR LEPTON PAIR PRODUCTION

The QCD perturbation processes in the hard scattering expansion are those involving nearly on mass shell QCD constituent of the beams, namely quarks, antiquarks, and gluons. The processes for lepton pair production are Compton and annihilation diagrams shown in Fig. 2. The calculations are the same as in QED with the addition of the color matrices and averaging factors.[3]

The $q+G \to \gamma^*+q'$ Compton diagrams Fig. 2(a) give the spin and color averaged matrix element squared

$$\bar{\Sigma}|\mathcal{M}|^2 = \left(\frac{1}{6}\right) e^2 q_i^2 g^2 \frac{2}{s(-t)} \left(u^2 + (Q^2)^2 - 2st\right) \tag{4.1}$$

where 1/6 is the color average and q_i the quark charge.

The annihilation diagrams $q+\bar{q} \to \gamma^*+G$ of Fig. 2(b) give the spin and color averaged matrix element squared

$$\bar{\Sigma}|\mathcal{M}|^2 = \left(\frac{4}{9}\right) e^2 q_i^2 g^2 \, 2\left(\frac{u}{t} + \frac{t}{u} + \frac{4Q^2 s}{tu}\right) \tag{4.2}$$

where 4/9 is the color factor.

V. PARTON CROSS SECTIONS

We first show how the production of a lepton pair of momentum Q integrated over lepton momentum $q_1+q_2=Q$ can be treated as the production of a massive virtual photon of mass squared Q^2 and wave function $\varepsilon_\mu(Q,\lambda)$. We then compute the pair differential cross section in the parton model from the matrix elements squared.

The cross section for production of a lepton pair from any scattering process B may be separated into the cross section for producing the virtual photon as a tensor $\Sigma^{\mu\nu}(B)$ times the photon propagator squared and lepton current squared $s_{\mu\nu} = 4(q_{1\mu}q_{2\nu} + q_{2\mu}q_{1\nu} - q_1 \cdot q_2 g_{\mu\nu})$. This

gives

$$\hat{\sigma} = \int \frac{d^3q_1}{2q_1^o} \int \frac{d^3q_2}{2q_2^o} \frac{s_{\mu\nu}}{(2\pi)^6} \frac{e^2}{(Q^2)^2} \int d\Phi_B \; \Sigma^{\mu\nu} \; \delta^4(q_1+q_2-P_B) \tag{5.1}$$

where P_B is the sum of all momentum in B other than the photon's and $d\Phi_B$ is the phase space. We introduce

$$1 = \int d^4Q \; \delta^4(q_1+q_2-Q) \int dQ'^2 \; \delta(Q'^2-Q^2)$$

remove the $\int dQ'^2$, convert $\int d^4Q \; \delta(Q'^2-Q^2) = \int d^3Q/2Q^o$ and use the result of the q_1 and q_2 integrals

$$\int \frac{d^3q_1}{2q_1^o} \int \frac{d^3q_2}{2q_2^o} \delta^4(q_1+q_2-Q) \; s_{\mu\nu} = \frac{2\pi Q^2}{3} \left(-g_{\mu\nu} + \frac{Q_\mu Q_\nu}{Q^2}\right)$$

$$= \frac{2\pi}{3} Q^2 \sum_\lambda \varepsilon_\mu(Q,\lambda) \; \varepsilon_\nu(Q,\lambda) \tag{5.2}$$

This gives the result

$$\frac{d\sigma^{\ell^+(q_1)\ell^-(q_2)}}{dQ^2} = \left(\frac{\alpha}{3\pi Q^2}\right) \int \frac{d^3Q}{2Q^o(2\pi)^2} \; d\Phi_B$$

$$\cdot \sum_\lambda \varepsilon_\mu \varepsilon_\nu \; \Sigma^{\mu\nu} \; \delta^4(q_1+q_2-P_B)$$

$$= \left(\frac{\alpha}{3\pi Q^2}\right) \sigma^{\gamma^*(Q)} \tag{5.3}$$

$\sigma^{\gamma^*(Q)}$ is the cross section to produce the virtual photon of mass squared Q^2. This holds for all differential cross sections in Q as well, such as

$$\frac{Q^o d\sigma^{\ell^+\ell^-}}{d^3Q dQ^2} = \left(\frac{\alpha}{3\pi Q^2}\right) \frac{Q^o d\sigma^{\gamma^*(Q)}}{d^3Q} \tag{5.4}$$

The parton model cross section for constituent a of beam A on constituent b of beam B is then

$$\frac{Q^0 d\sigma}{d^3Q dQ^2} = \left(\frac{\alpha}{3\pi Q^2}\right) \int dx_a \int dx_b \; P_{a/A}(x_a) \; P_{b/B}(x_b)$$

$$\cdot \frac{1}{16\pi^2 s} \delta(s+t+u - Q^2 - \Sigma p^2) \; \bar{\Sigma} |\mathcal{M}|^2$$

VI. KINEMATICS WITH OFF-SHELL PARTONS

We present an exact treatment of the kinematics of the hard scattering process allowing the squared momenta of the partons to be off mass shell at arbitrary values.[8] We also do the dx_b integral exactly. The kinematic restriction $s+t+u = Q^2 + \Sigma p^2$ leads in general to a quadratic relation between x_a and x_b. We show a special case in which this becomes linear. For our calculations we keep initial partons spacelike and expand the kinematics for large Q^2 and s.

The key to allowing arbitrary parton momentum squared is not to overconstrain incoming parton momenta p_a, p_b by relating them to beam momenta P_a, P_b by $p_a = x_a P_a$, $p_b = x_b P_b$. Instead we use the boost invariant relations or light cone variables with $p^{\pm} \equiv p^0 \pm p_Z$: $p_a^+ = x_a P_a^+$, $p_b^- = x_b P_b^-$ where P_a is along the positive Z direction. The energy momentum relation for the hard scattering $p_a + p_b = Q + q'$ is

$$s+t+u = Q^2 + q'^2 + p_a^2 + p_b^2 \tag{6.1}$$

We define externally set ratios

$$x_+ = \frac{Q_+}{P_a^+}, \qquad x_- = \frac{Q_-}{P_a^-}, \qquad x_+ x_- = \frac{Q^2 + Q_\perp^2}{P_a^+ P_b^-} \tag{6.2}$$

scaling variables,

$$z_a = \frac{x_a}{x_+}, \qquad z_b = \frac{x_b}{x_-}, \qquad r_\perp = \frac{Q_\perp^2+q'^2}{Q^2+Q_\perp^2} \tag{6.3}$$

and small ratios

$$\varepsilon_a = \frac{p_a^2}{Q_\perp^2+Q_\perp^2}, \qquad \varepsilon_b = \frac{p_b^2}{Q^2+Q_\perp^2} . \tag{6.4}$$

The hard scattering invariants are then

$$\begin{aligned} s &= \left(Q^2+Q_\perp^2\right)(z_a z_b + \varepsilon_a + \varepsilon_b + \varepsilon_a\varepsilon_b/(z_a z_b)) \\ t &= Q^2 - \left(Q^2+Q_\perp^2\right)(z_a - \varepsilon_a(1-1/z_a)) \\ u &= Q^2 - \left(Q^2+Q_\perp^2\right)(z_b - \varepsilon_b(1-1/z_b)) \end{aligned} \tag{6.5}$$

The kinematic relation (6.1) becomes a quadratic relation between z_a and z_b or x_a and x_b.

$$\left(z_b - 1 + \frac{\varepsilon_a}{z_b}\right)\left(z_a - 1 + \frac{\varepsilon_b}{z_b}\right) = r_\perp \tag{6.6}$$

The essential point of keeping the squared momenta is to show the source of the cutoff as $t \propto -Q_\perp^2 \to 0$. To do this we convert from z_a to t and look at the upper t_{up} limit as $Q_\perp \to 0$. The minimum z_a and $|t|$ occur at the maximum $x_b=1$, $z_b=1/x_-$. Expanding to first order in ε_a and ε_b

$$t_{up} = -\frac{Q_\perp^2}{1-x_-} - \frac{x_-}{1-x_-}\left[q'^2 - p_b^2(1-x_-) - p_a^2\frac{Q^2}{Q^2+Q_\perp^2(1-x_-)}\right] \tag{6.7}$$

The integral over dx_b can be done using the δ function and the dx_a integral converted to dt by expanding in ε_a, ε_b to get to zeroth

order

$$\int dx_a \int dx_b \; \delta\left(s+t+u - Q^2 - p_a^2 - p_b^2 - q'^2\right)$$
$$= \int_{t_{low}}^{t_{up}} dt \left[-t - Q_\perp^2 + p_b^2\left(\frac{-t - Q_\perp^2}{-t + q'^2}\right)\right]^{-1} \tag{6.8}$$

We see that at $Q_\perp=0$ we are saved from a t=0 singularity by the presence of the virtual parton momenta squared in t_{up}. At $Q_\perp \cong 0$ and x_- small, (6.7) has the form then

$$t_{up} \cong \frac{-Q_\perp^2 - x_-\kappa}{1-x_-} \tag{6.9}$$

where

$$\kappa \cong q'^2 - p_b^2 - p_a^2 \tag{6.10}$$

We can crudely relate the off mass shell values to an intrinsic parton transverse momentum. From a similar calculation to that which led to (6.7) we expect the incoming quarks to have spacelike four momenta with $p_a^2 \sim -\langle(p_\perp^2 + x\tilde{m}^2)/(1-x)\rangle$ where $\tilde{m}$ is the effective mass of the spectator system. The incoming $q\bar{q}$ or qq "mesons" have $\langle p_\perp^2\rangle_M = \langle(p_{1\perp}+p_{2\perp})^2\rangle = 2\langle p_\perp^2\rangle_q$ and $p_b^2 \sim -2\langle(p_\perp^2+x\tilde{m}^2)/(1-x)\rangle$. The outgoing quark "decays" into a quark jet with the $p_\perp$ of a quark in the jet hadrons and may be expected to have a timelike q'^2 of the same order as a quark $(-p_a^2)$. The value of κ used to fit the μ pair data presented later is $\kappa \simeq 2$ GeV^2. This then corresponds roughly to $\langle(p_\perp^2+x\tilde{m}^2)/(1-x)\rangle \sim 0.5$ GeV^2 and is consistent with $\tilde{m}^2 \sim 1$ GeV^2, $\langle p_\perp^2\rangle \sim .1$ GeV^2 and $x \sim 1/3$. Other than the significant off mass shell kinematic effects, we have not taken into account the small parton $p_\perp$ smearing before the hard scattering process. The effects of the smearing are reportedly small with off mass shell kinematics.[10]

The equation (6.6) can be solved linearly only in the case $\epsilon_a = \epsilon_b = 0$. The result still depends on q'^2 through $r_\perp$. However, the general expansion of (6.6) and (6.5) to first order in ϵ_a and ϵ_b puts $-p_a^2$ and $-p_b^2$ mass factors in the same places as q'^2 as seen in Eq. (6.7) for example.

So for simplicity we can use the exact linear results of setting $\epsilon_a=0$, $\epsilon_b=0$, by replacing q'^2 with $\kappa \simeq 2$ GeV^2.

In terms of t, the variables constrained by the δ function are then simply

$$x_a = x_+ \left(\frac{Q^2 - t}{Q^2 + Q_\perp^2}\right), \qquad x_b = x_- \left(\frac{-t + \kappa}{-t - Q_\perp^2}\right)$$

$$s = \frac{(-t+Q^2)(-t+\kappa)}{(-t - Q_\perp^2)} \tag{6.11}$$

$$u = \frac{-Q_\perp^2(Q^2-t+\kappa) - \kappa Q^2}{(-t - Q_\perp^2)}$$

VII. CROSS SECTION CALCULATIONS

We now present the results of the calculations of the preceding QCD and CIM contributions to the cross sections. We concentrate mainly on the Columbia-Fermilab-Stony Brook[11] (CFS) muon pair data at $\sqrt{s} = 27.4$ GeV and 5 GeV/c^2 < M < 15 GeV/c^2. We then project results to proton-proton colliding rings and discuss the deviations from scaling.

The following parton distributions are used[12]

$$P_{u/P}(x) = 1.79(1-x)^3\ (1+2.3x)/\sqrt{x} + s(x)$$

$$P_{d/P}(x) = 1.107(1-x)^{3.1}/\sqrt{x} + s(x)$$

We use the sea distribution from Drell-Yan used by CFS[11] in order to compare with other QCD calculations

$$s(x) = 0.6(1-x)^{10}/x$$

We have also used the sea from lepton-hadron experiments

$$s(x) = 0.15(1-x)^{7}/x$$

Since the antiquarks predominantly come from the meson system, this difference of seas is only a few percent in the CIM results. The gluon distribution consistent with ψ and Υ production[13] and the momentum sum rule is

$$G(x) = 3(1-x)^{5}/x$$

The meson distribution inside a proton consistent in magnitude with the height of the central plateau is

$$P_{M/P}(x) = 2.5\ (1-x)^{7}/x$$

where the power is determined by fitting $d\sigma/dMdy$ at high $\sqrt{\tau} = M/\sqrt{s}$.

A. QCD Perturbation Theory

The calculation of the QCD Compton graphs (Fig. 2(a)) and Eq. (4.1) is presented in Fig. 4(a) for $M = 5.5$ GeV/c^2 at $\sqrt{s} = 27.4$ GeV. The upper curve is calculated with no off mass shell kinematic cutoff and diverges as $Q_\perp \to 0$. The lower curve is calculated using the off mass shell kinematics with $\kappa = 2$ GeV^2. The off shell kinematics not only remove the $Q_\perp \to 0$ divergence but also cut down the contribution by more than a factor of two for $Q_\perp < 1.5$ GeV/c.

The calculation of the QCD annihilation graphs (Fig. 2(b)) and Eq. (4.2) is shown in Fig. 4(b) at the same parameters as in Fig. 4(a). The values of the annihilation and Compton diagrams with cutoffs are of similar magnitude at low $Q_\perp < 1.5$ GeV/c but the annihilation falls off faster

in $x_\perp = Q_\perp/(Q_\perp)_{max}$ because the antiquark sea distribution $(1-x)^{10}$ is much steeper than the gluon distribution $(1-x)^5$.

The curves with no cutoff agree with those of Ref. 14 but are roughly a factor of 3 below those of Ref. 15.

Since the perturbative QCD sum is about 1/6 of the data at $M \sim 5$-8 GeV/c^2, we compute the non-perturbative contribution next.

B. Bound State Contribution

The bound state contribution from the diagrams of Fig. 1 and Eq. (3.6) are the dominant contribution to the cross section. We fit the differential $Q_\perp$ cross section using this contribution plus the smaller QCD contribution. The fits to $d\sigma/dMdyd^2Q_\perp$ at y=0 are shown in Fig. 5(a,b). The quantities $\langle Q_\perp \rangle$, $\langle Q_\perp^2 \rangle$ are most sensitive to the off mass shell value and determine $\kappa \gtrsim 2$ GeV^2, $m^2 \gtrsim 2$ GeV^2 and $m_b^2 \simeq 2$ GeV^2. Good fits can be obtained for a wide range of λ and those shown are for $\lambda = 1/2$. The coupling strength that fits the data is best expressed as the coefficient $m^2 g_M^2$ of the extra $1/k^2$ behavior of the bound state form factor squared at large $k^2 \gtrsim -Q_\perp^2$. The fit gives $A^2 \equiv g_M^2 m^2/3 = 58$ GeV^2. This is in excellent agreement with $A^2 = 55$ GeV^2 used to fit the $p_\perp^{-8}$ behavior of the single pion spectrum in our earlier paper.[2]

The fit to the data for the coefficient A^2 must include all effective "meson" channels n_{eff}. If we interpret the "meson" simply as any $q\bar{q}$ inside the incoming hadron, then the calculation above was for only the pseudoscalar S=0 spin combination. If the three S=1 states give a similar contribution, we have $n_{eff}=4$. We now compare with the

normalization of all CIM processes.[16] This is in terms of

$$\alpha_M \equiv \frac{1}{3}\frac{m^2 g_M^2}{4\pi} = \frac{A^2}{4\pi}\frac{1}{n_{eff}} = 1.2$$

and agrees with $\alpha_M \approx 1$ found in the CIM processes.[16]

In Fig. 6 is the fit to $d\sigma/dMdy$ data[11] at $\sqrt{s}$ = 27.4 GeV using the sum of CIM, Compton, and annihilation contributions. We also show the Compton and annihilation contributions separately.

In Fig. 7 are the differential cross sections projected to higher $Q_\perp$ values showing QCD versus CIM. At sufficiently high $Q_\perp > 6$ GeV the scaling $1/Q_\perp^4$ behavior of QCD emerges dominant over the $m^2/Q_\perp^6$ behavior of CIM.

In Fig. 8 are shown[11] $\langle Q_\perp \rangle$ and $\langle Q_\perp^2 \rangle$ at $\sqrt{s}$ = 27.4 GeV and y=0 as solid lines. The calculation of $\langle Q_\perp \rangle$ with a cutoff at $Q_\perp$ = 4 GeV/c, as in the data,[11] is about the same but the calculation of $\langle Q_\perp^2 \rangle$ with a 4 GeV/c cutoff is lower and shown with a dashed line. The fits are compared with the data. In Fig. 8(b) we show the expected $\langle Q_\perp \rangle$ at the ISR $\sqrt{s}$ = 53 GeV and Isabelle $\sqrt{s}$ = 800 GeV energies compared with Fermilab $\sqrt{s}$ = 27.4 versus $M/\sqrt{s}$. The large values of $\langle Q_\perp \rangle$ at higher energy is due to the emergence of the QCD contributions.

In Fig. 9 we show the scaled cross section $M^3 d\sigma/dMdy\big|_{y=0}$ at different energies and $M/\sqrt{s}$ for pp collisions. Due to the virtual masses present in determining the shape of the $Q_\perp$ spectra, the curves do not show exact Drell-Yan scaling at fixed $M/\sqrt{s}$, but come within a factor of $\sim$10 from $\sqrt{s}$ = 20 to 800 GeV. This is approximate scaling since the cross section $d\sigma/dMdy$ varies by $(20)^3 \sim 10^4$ over this range. These curves are shown only to illustrate these effects and are not good as predictions since

the QCD scaling violations in the structure functions will give significant decreases at these large M^2.

In Fig. 10 we examine the scaled cross sections $Q_\perp^2 M^3 d\sigma/dMdy\big|_{y=0}$ for pp collisions to show the emergence of the QCD scaling contribution from the CIM contribution which behaves like an extra 1/s at fixed $x_\perp = Q_\perp/\sqrt{s}$ and fixed $M/\sqrt{s} = 0.1$.

One of us (D.S.) would like to thank the Stanford Linear Accelerator Center for its hospitality and R. Blankenbecler, S. Brodsky, S. Drell, P. Lepage, R. Horgan and P. Scharbach for discussions. We would also like to thank the Aspen Center for Physics for its hospitality.

REFERENCES

1. M. Duong-van, K. V. Vasavada, and R. Blankenbecler, Phys. Rev. D 16, 1389 (1977).
2. C. M. Debeau and D. Silverman, University of California Irvine preprint 77-28, Phys. Rev. D, to be published.
3. H. D. Politzer, Nucl. Phys. B129, 301 (1977).
4. D. Sivers, S. J. Brodsky, and R. Blankenbecler, Phys. Reports 23C, 1 (1976).
5. R. M. Barnett and D. Silverman, Phys. Rev. D 10, 1510 (1974).
6. M. Bander, R. M. Barnett, and D. Silverman, Phys. Lett. 48B, 243 (1974).
7. D. Jones and J. F. Gunion, Stanford Linear Accelerator Center preprint SLAC-PUB-2157 (1978).
8. W. E. Caswell, R. R. Horgan, and S. J. Brodsky, Stanford Linear Accelerator Center preprint SLAC-PUB-2106 (1978).
9. S. D. Drell and T. D. Lee, Phys. Rev. 5, 1738 (1972); J. D. Bjorken and S. D. Drell, Relativistic Quantum Mechanics (McGraw-Hill, New York, 1964).
10. R. R. Horgan and P. N. Scharbach, Stanford Linear Accelerator Center preprint SLAC-PUB-2188 (1978).
11. D. M. Kaplan et al., Phys. Rev. Lett. 40, 435 (1978).
12. R. McElhaney and S. F. Tuan, Phys. Rev. D 8, 2267 (1973).
13. C. E. Carlson and R. Suaya, Phys. Rev. Lett. 39, 908 (1978).
14. E. L. Berger, Argonne National Laboratory preprint ANL-HEP-PR-78-12 (1978);

15. F. Halzen and D. M. Scott, Phys. Rev. Lett. 40, 1117 (1978) and University of Wisconsin COO-881-21 (1978).

16. R. Blankenbecler, S. J. Brodsky, and J. F. Gunion, Phys. Rev. D 18, 900 (1978).

FIGURE CAPTIONS

1. Quark-meson diagrams for lepton pair production with form factors. The dashed lines are gluons and the circles represent a full non-perturbative sum.
2. QCD contributions to lepton pair production. (a) Compton graphs for quark-gluon scattering to lepton pairs. (b) quark-antiquark annihilation to lepton pairs.
3. Off shell $q\bar{q}M$ vertex in the single gluon exchange approximation.
4. (a) QCD Compton graph results with off mass shell kinematic cutoff and without the cutoff. (b) QCD annihilation graph results with and without cutoff.
5. Muon pair production cross sections $d\sigma/dMdyd^2Q_\perp$ from Ref. 11 and fits with CIM plus QCD in pair mass intervals (a) M = 5.5 GeV, 7.5 GeV, and (b) M = 6.5 GeV, 8.5 GeV, at $\sqrt{s}$ = 27.4 GeV.
6. Muon pair cross section $d^2\sigma/dMdy$ from Ref. 11 at $\sqrt{s}$ = 27.4 GeV and fit with CIM plus Compton and annihilation graphs (solid line). Also shown is the Compton result alone (dashed line) and the annihilation result (dotted line) with the off mass shell kinematics.
7. Muon pair cross section $d\sigma/dMdyd^2Q_\perp$ at y=0 for higher $Q_\perp$ values showing separately the contributions of the CIM (solid line), the Compton graphs (dashed line) and the annihilation graphs (dotted line).
8. (a) Values of $\langle Q_\perp \rangle$ (circles) and $\langle Q_\perp^2 \rangle$ (boxes) from Ref. 11 at $\sqrt{s}$ = 27.4 GeV. The solid lines are fits integrating over all allowed $Q_\perp$. The dashed line is the fit to $\langle Q_\perp^2 \rangle$ cutting off at $Q_\perp \leq 4$ GeV. (b) $\langle Q_\perp \rangle$ at various energies using the same parameters as fit (a).

9. Scaled cross sections $M^3 d\sigma/dMdy$ showing the effects of different energies.

10. Variation with energy of scaled CIM and QCD cross sections at fixed $x_\perp = Q_\perp/\sqrt{s}$ and fixed $M/\sqrt{s}$ showing the extra 1/s falloff of CIM and the approach to scaling with off shell kinematics.

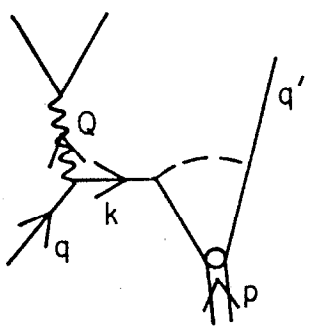

(a) t-channel

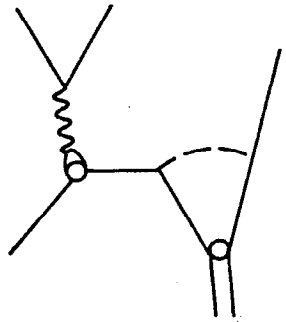

(b) Q^2-channel

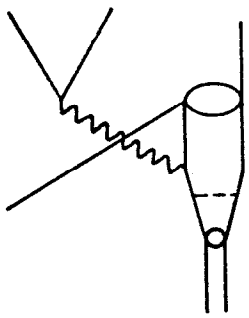

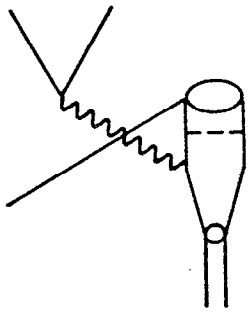

8-78

(c) u-channel

3455A1

Fig. 1

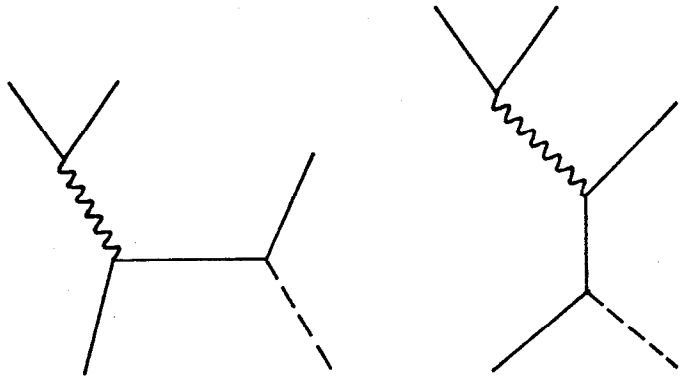

(a) Compton

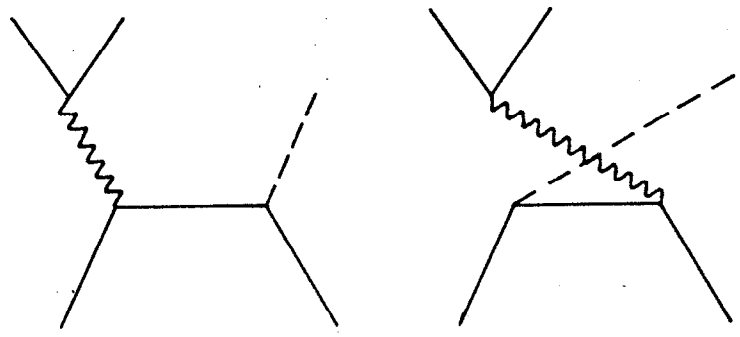

8-78 (b) Annihilation 3455A2

Fig. 2

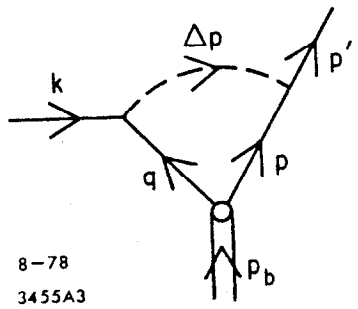

Fig. 3

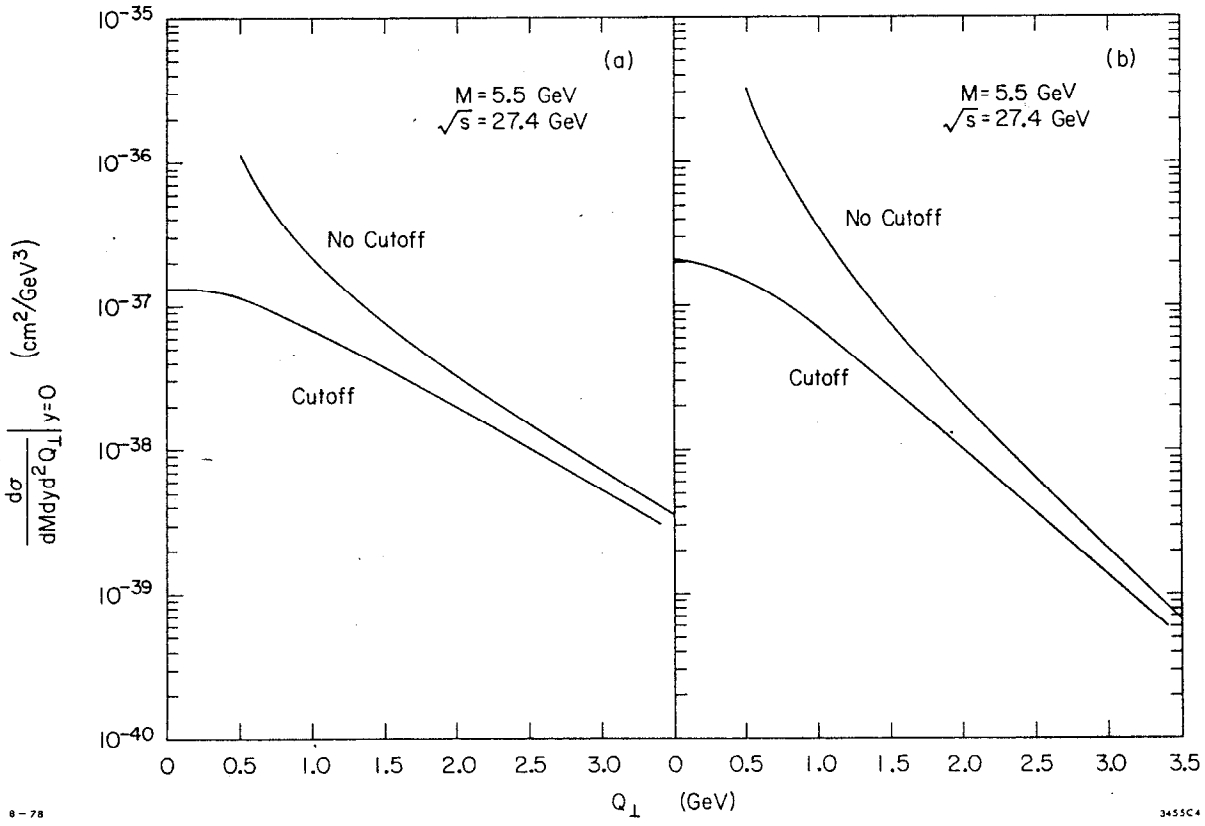
(a)
M = 5.5 GeV
√s = 27.4 GeV
No Cutoff
Cutoff
(b)
M = 5.5 GeV
√s = 27.4 GeV
No Cutoff
Cutoff
10^-35
10^-36
10^-37
10^-38
10^-39
10^-40
dσ/dMdyd²Q⊥ |y=0 (cm²/GeV³)
0
0.5
1.0
1.5
2.0
2.5
3.0
0
0.5
1.0
1.5
2.0
2.5
3.0
3.5
Q⊥ (GeV)
8-78
3455C4

Fig. 4

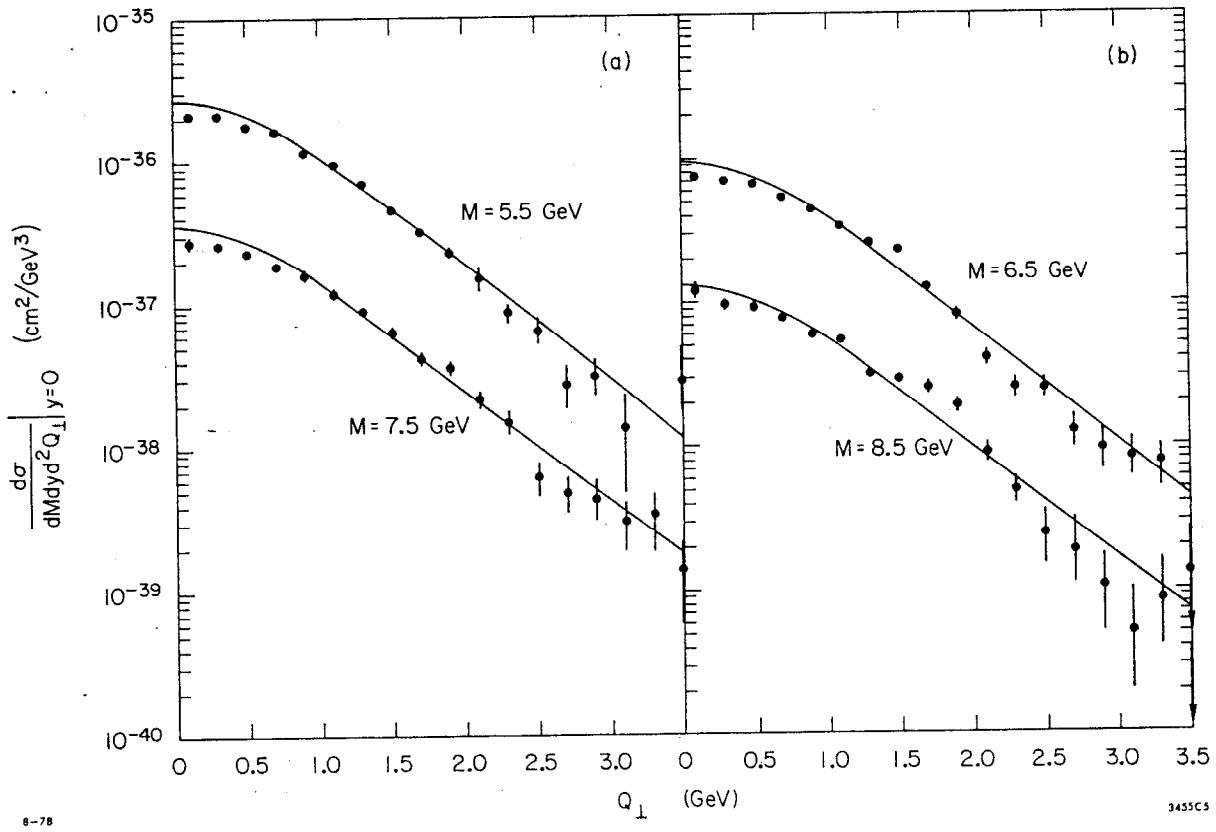
(a)
(b)
M = 5.5 GeV
M = 7.5 GeV
M = 6.5 GeV
M = 8.5 GeV
$\frac{d\sigma}{dMdyd^2Q_\perp}\Big|_{y=0}$ (cm²/GeV³)
$Q_\perp$ (GeV)
8-78
3455C5

Fig. 5

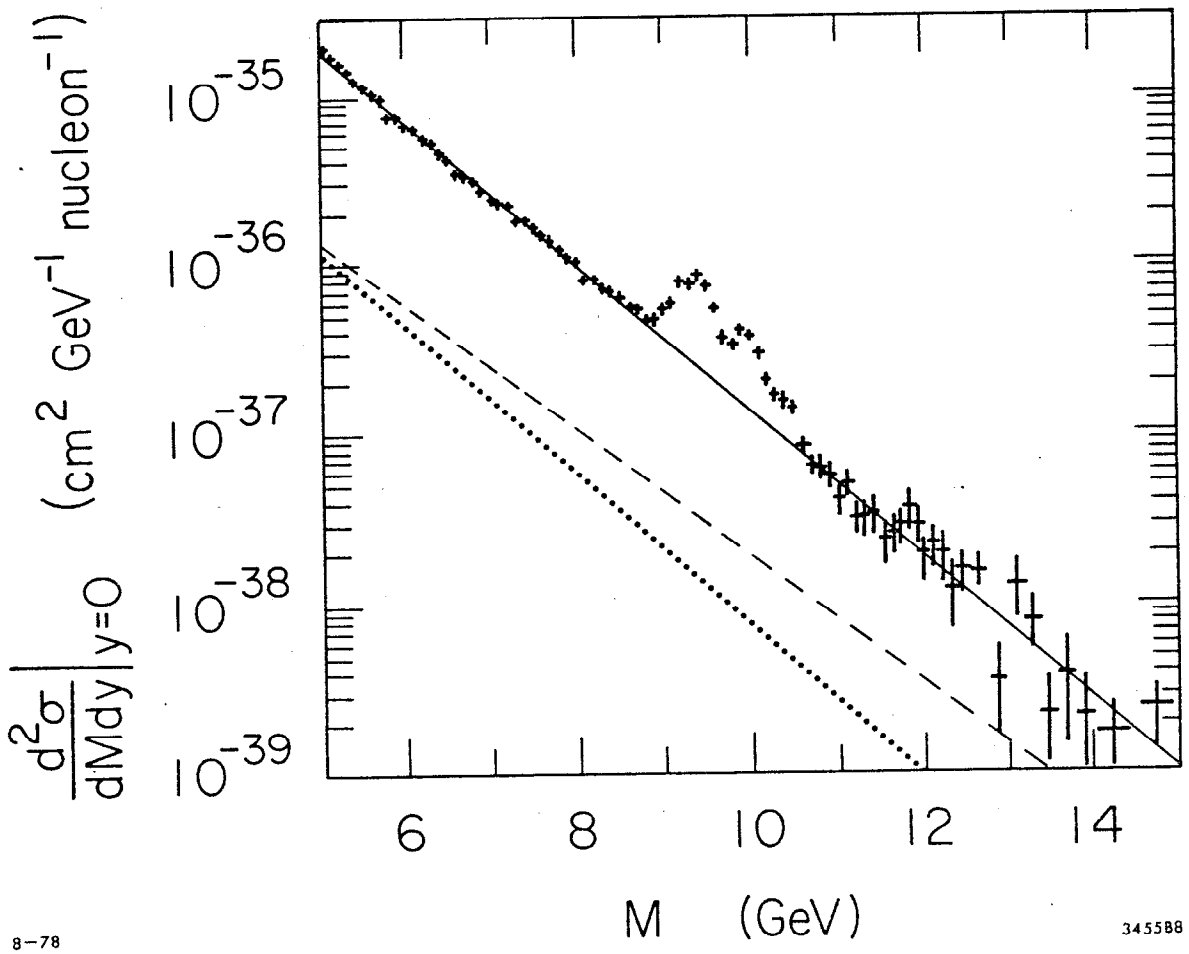
$\frac{d^2\sigma}{dMdy}\Big|_{y=0}$ (cm^2 GeV^{-1} nucleon^{-1})
10^{-35}
10^{-36}
10^{-37}
10^{-38}
10^{-39}
6
8
10
12
14
M (GeV)
8-78
345588

Fig 6

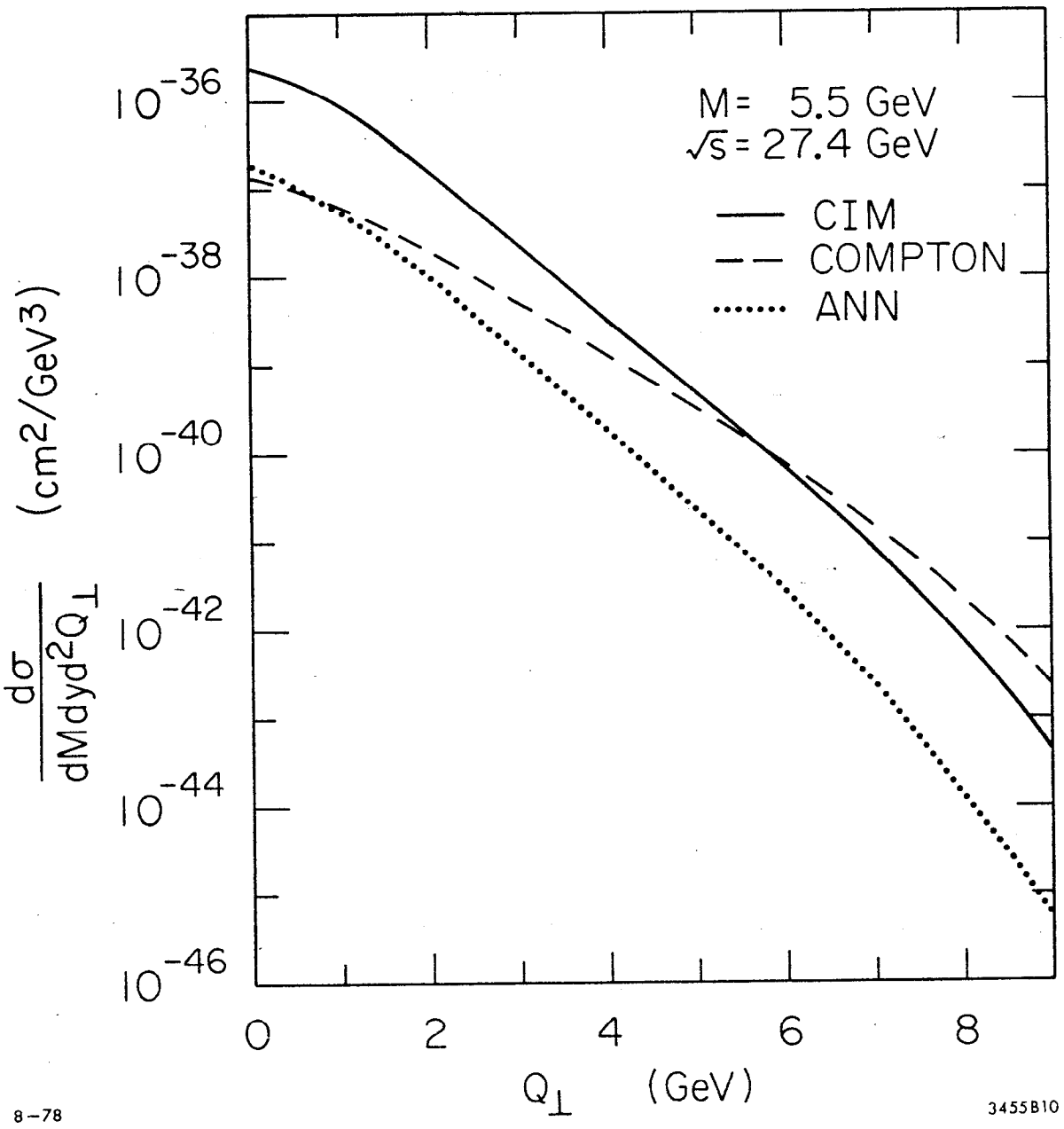
M= 5.5 GeV
√s = 27.4 GeV
CIM
COMPTON
ANN
10^{-36}
10^{-38}
10^{-40}
10^{-42}
10^{-44}
10^{-46}
$\frac{d\sigma}{dMdyd^2Q_\perp}$ (cm²/GeV³)
0
2
4
6
8
$Q_\perp$ (GeV)
8–78
3455B10

Fig. 7

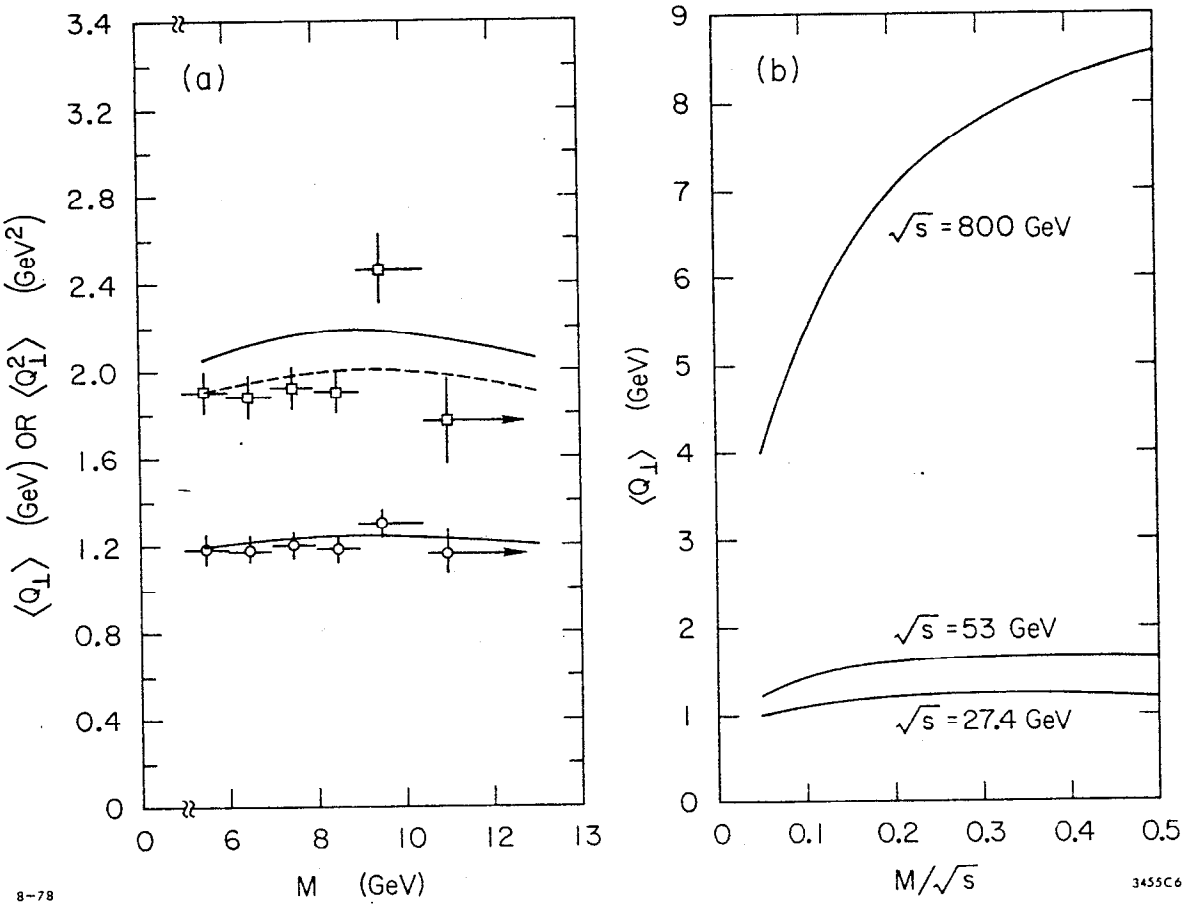
(a)
(b)
$\langle Q_\perp \rangle$ (GeV) OR $\langle Q_\perp^2 \rangle$ (GeV^2)
M (GeV)
$\langle Q_\perp \rangle$ (GeV)
$M/\sqrt{s}$
$\sqrt{s}$ = 800 GeV
$\sqrt{s}$ = 53 GeV
$\sqrt{s}$ = 27.4 GeV
8-78
3455C6

Fig. 8

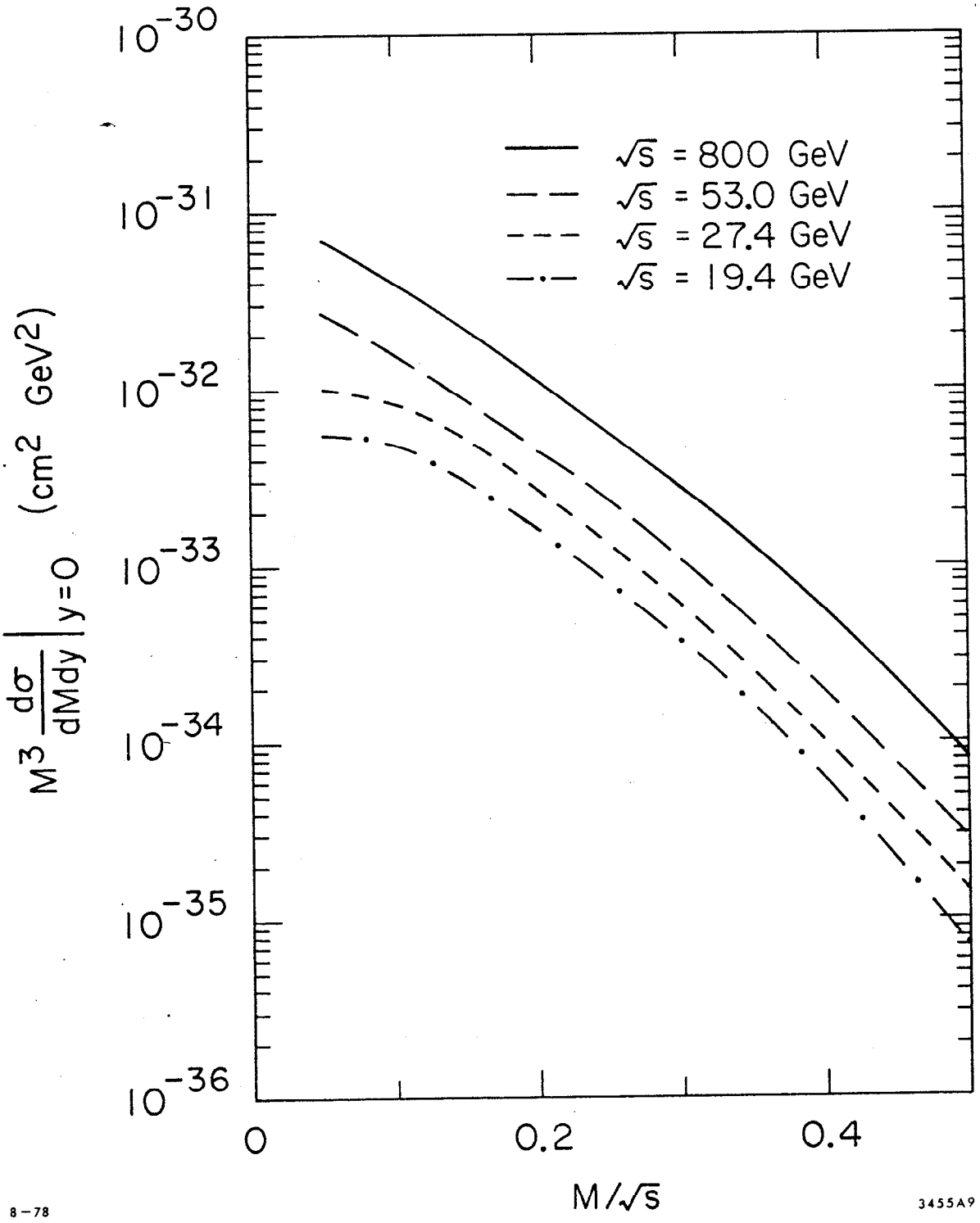
10^{-30}
10^{-31}
10^{-32}
10^{-33}
10^{-34}
10^{-35}
10^{-36}
$M^3 \frac{d\sigma}{dMdy}\Big|_{y=0}$ (cm^2 GeV^2)
$\sqrt{s}$ = 800 GeV
$\sqrt{s}$ = 53.0 GeV
$\sqrt{s}$ = 27.4 GeV
$\sqrt{s}$ = 19.4 GeV
0
0.2
0.4
$M/\sqrt{s}$
8-78
3455A9

Fig. 9

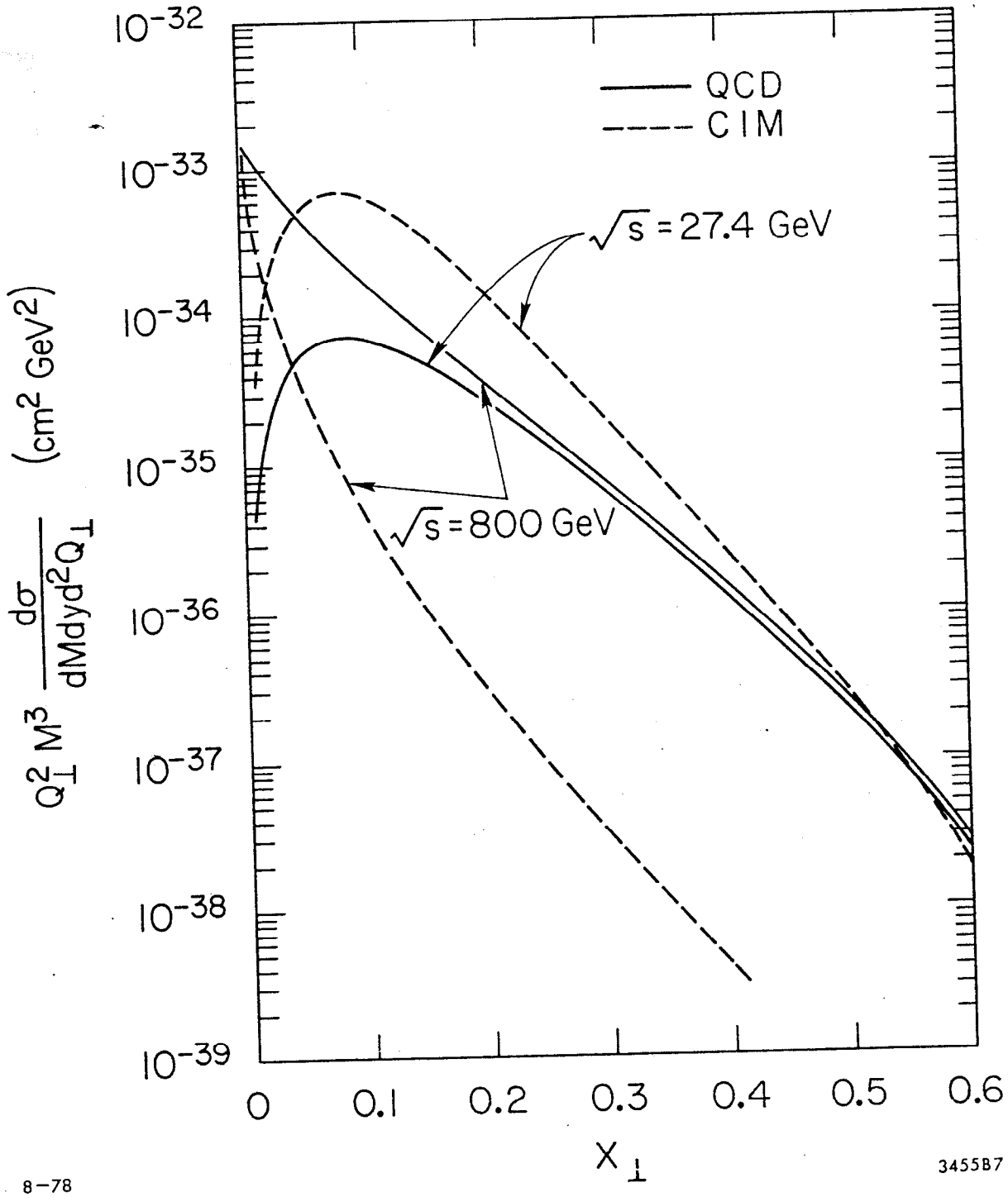
QCD
CIM
$\sqrt{s}$ = 27.4 GeV
$\sqrt{s}$ = 800 GeV
$Q_\perp^2 M^3 \frac{d\sigma}{dMdyd^2Q_\perp}$ (cm^2 GeV^2)
10^{-32}
10^{-33}
10^{-34}
10^{-35}
10^{-36}
10^{-37}
10^{-38}
10^{-39}
0
0.1
0.2
0.3
0.4
0.5
0.6
$X_\perp$
8-78
3455B7

Fig. 10